Observational Study

Medicine®

OPEN

Early white matter injuries in patients with acute carbon monoxide intoxication

A tract-specific diffusion kurtosis imaging study and STROBE compliant article

Ping-Huei Tsai, PhD[a,b,c], Ming-Chung Chou, PhD[d], Shih-Wei Chiang, MS[e], Hsiao-Wen Chung, PhD[f], Hua-Shan Liu, PhD[b,c,g], Hung-Wen Kao, MD[e], Cheng-Yu Chen, MD[a,b,c,e,*]

Abstract

Evaluation of acute white matter injuries caused by carbon monoxide (CO) poisoning can be limited by conventional magnetic resonance (MR) imaging. We aim to evaluate the feasibility of diffusion kurtosis imaging (DKI) for early detection of white matter alterations in patients with acute CO intoxication.

A total of 30 subjects including 15 acute CO patients and 15 age- and sex-matched healthy volunteers were enrolled in this study. MR examinations were performed on a 3T MR scanner within 8 days after CO intoxication. DKI data were acquired to derive axial, radial, and mean kurtosis, as well as fractional anisotropy (FA), axial, radial, and mean diffusivity for tract-specific comparisons between the 2 groups.

Significant decreases of mean kurtosis were shown in the genu of corpus callosum, cingulum, and motor-related tracts (corticospinal and corticobulbar tracts) in patients with acute CO intoxication as compared with controls. On the contrary, significant differences of FA values were merely shown in the regions of corticospinal tracts.

DKI demonstrated comparably stronger potential than diffusion tensor imaging in terms of early detection of white matter changes in patients with acute CO intoxication. This may have implications in therapeutic strategy for managing acute CO intoxication patients.

Abbreviations: CO = Carbon monoxide, COHb = Carboxyhemoglobin, DKI = Diffusion kurtosis imaging, DTI = Diffusion tensor imaging, FA = Fractional anisotropy, HBOT = Hyperbaric oxygen therapy, MD = Mean diffusivity, MK = Mean kurtosis.

Keywords: acute CO intoxication, DKI, DTI, FA, MK, non-Gaussian

1. Introduction

Carbon monoxide (CO) intoxication has frequently been the results of attempted suicide by charcoal burning in Taiwan, which often result in substantial neuropsychiatric complications.[1] The common sequelae include parkinsonism, motor impairments, cognitive, and memory deficits that may occur within 2 to 3 weeks after CO exposure.[2,3] Hyperbaric oxygen therapy (HBOT) has been used as the treatment after CO poisoning; however, the neuropsychological sequelae accompanied with delayed encephalopathy could still be estimated to occur in up to 47% of the patients and may persist for weeks or longer even with HBOT.[4] Although the pathophysiologic mechanism remains unclear, a previous report indicated that inhibited cellular energy metabolism even after normalization of carboxyhemoglobin (COHb) levels may explain the progressive neuropsychiatric impairments of the patients after HBOT.[5]

To determine the risk of delayed encephalopathy, numerous studies have focused on assessing the relationship between the radiological finding of brain abnormalities and neuropsychiatric outcomes following CO poisoning using magnetic resonance imaging (MRI) and computed tomography (CT).[6,7] Acute necroses with low-density changes in the globus pallidi on CT images were demonstrated in patients after CO poisoning who had delayed encephalopathy and white matter lesions following 2 to 26 weeks of latency.[8] Moreover, diffuse and progressive white matter (WM) hyperintensity on diffusion-weighted MR image and FLAIR image was observed to extend to subcortical WM in 1 to 3 months after CO exposure, suggestive of demyelination.[9] Those reported macrostructural discrepancies on the images of the patients are characterized in relatively late stages, resulting in reduced opportunity for alleviating the neuropsychiatric deficits after acute insult. Consequently, early

Editor: Bernhard Schaller.

Funding: This study was supported in part by grants from Tri-Service General Hospital and National Defense Medical Center (TSGH-C102-048, Chen CY), Taipei Medical University (TMU103-AE1-B34, Tsai PH, TMU103-AE1-B29, 104TMU-TMUH-03, Liu HS), and Ministry of Science and Technology of Taiwan (NSC 98–2314-B-016–022-MY2, Chen CY, MOST 105-2221-E-038-006, Tsai PH).

[a] Department of Radiology, School of Medicine, College of Medicine, Taipei Medical University, [b] Translational Imaging Research Center, [c] Department of Medical Imaging, Taipei Medical University Hospital, Taipei Medical University, Taipei, [d] Department of Medical Imaging and Radiological Sciences, Kaohsiung Medical University, Kaohsiung, [e] Department of Radiology, Tri-Service General Hospital and National Defense Medical Center, [f] Graduate Institute of Biomedical Electronics and Bioinformatics, National Taiwan University, [g] School of Biomedical Engineering, College of Biomedical Engineering, Taipei Medical University, Taipei, Taiwan.

[*] Correspondence: Cheng-Yu Chen, Department of Medical Imaging, Taipei Medical University Hospital, Taipei Medical University, No.252, Wu Hsing Street, Taipei City 110, Taiwan (R.O.C.) (e-mail: sandy0932@gmail.com).

Medicine (2017) 96:5(e5982)

Received: 8 December 2015 / Received in final form: 3 January 2017 / Accepted: 4 January 2017

http://dx.doi.org/10.1097/MD.0000000000005982

radiological detection of subtle changes of WM microstructures due to CO intoxication should be urgently needed.

With the ability to reveal changes in brain tissue integrity in vivo noninvasively, tremendous reports have utilized diffusion tensor imaging (DTI)-derived parameters to characterize delayed encephalopathy after CO intoxication.[10,11] Decreased fractional anisotropy (FA) of specific WM tracts was found in patients after acute CO intoxication, confirming the occurrence of WM changes,[12,13] which in turn exhibits potential for predicting the clinical outcome.[14] However, the behavior of water signal decay on diffusion-weighted images in neuronal tissues is known to be highly sophisticated.[15,16] Appropriate description of that could reveal additional microstructural information in which the slow diffusion component is suggestively associated with neuronal maturation,[17] implying some room for improvements of the DTI method for early depiction of microstructural alterations.

Recently, diffusion kurtosis imaging (DKI) has been proposed to characterize the non-Gaussian water diffusion and quantify the degree of diffusion restriction in neural tissues.[18–20] With DKI, not only the conventional DTI parameters are derivable, but also complexity and heterogeneity of the microenvironments could also be distinguished, thereby indicating the potential of being a more sensitive biomarker than DTI to brain pathophysiological changes.[20–23] We hypothesize that DKI can be beneficial in improving the early depiction of delayed encephalopathy in patients after acute CO intoxication. Therefore, we aim to evaluate the feasibility of DKI for early detection of white matter alterations in patients with acute CO intoxication.

2. Methods

2.1. Subjects

This study was approved by the Institutional Review Board of National Defense Medical Center (Approval number TSGHIRB-2-101-05-048) in Taipei, Taiwan. All participants were recruited in this preliminary study between January 2013 and March 2015 after obtaining written informed consent. Patients who had a positive history of acute CO intoxication and presented with acute toxic signs at the emergency department and the measurements of carboxyhemoglobin levels were available and included in this study. As a result, 15 patients (5 males and 10 females, average age 38.7 ± 11.4 years) with acute CO intoxication were recruited, with another 15 age- and gender-matched normal volunteers (average age 39.4 ± 12.0 years) as control. None of the control participants had a history of neurological disease or neuropsychiatric disorder. Patients with previous use of neuroleptics, a family history of demyelinating diseases or Parkinsonism, a history of stroke, or encephalitis were excluded. Those who have a history of head injury or surgery, whose clinical findings showing trauma or subacute CO intoxication, and whose images showing severe motion artifacts were also excluded. The total number of 30 subjects reflected the results after exclusion. Four out of 15 patients were smokers. The measured COHb levels of the patients before HBOT were 26.21 ± 15.93%. The mean COHb level in the control group is less than 1.5%. All patients underwent MRI within 8 days (averaged period 5.20 ± 2.23 days) after the CO poisoning event.

2.2. MR imaging

All MRI was performed on a 3.0T MR scanner (Discovery MR750; GE Healthcare, Milwaukee, WI). After image acquisitions using the conventional imaging protocols (T1-weighted, T2-weighted, and FLAIR images), DKI data were obtained using spin echo diffusion-weighted 2D EPI imaging with b values of 0, 1000, and 3000 s/mm^2 in 40 noncollinear directions. Other imaging parameters were as follows: TR/TE = 10,000/110.5 ms, FOV = 240 × 240 mm^2, matrix size = 128 × 128 (zero-filled to 256 × 256), slice thickness = 4 mm, number of slices = 36, ASSET = 2, bandwidth = 1953.12 Hz/Pixel. Furthermore, 3D T1-weighted images were acquired using fast SPGR sequence with TR = 10.2 ms; TE = 4.2 ms; Flip angle = 12°; FOV = 256 × 256 mm^2, matrix size = 256 × 196 (zero-filled to 256 × 256), slice thickness = 1 mm, number of slices = 143, bandwidth = 162.73 Hz/Pixel. Total scan time was less than 40 minutes. Moreover, DKI data acquisition was performed in 2 sessions (scan and rescan) on 3 out of 15 normal subjects to test the reproducibility of the proposed method.

2.3. Data analysis

After data acquisition, the images were processed using an in-house script implemented in MATLAB (MathWork, Natick, MA) based on the algorithm proposed by Tabesh et al.[24] The detailed information was as follows: Mis-registrations from eddy current and/or involuntary motions were first corrected using an affine registration scheme, followed by a pre-processing step of median filtering to alleviate the noise effect on DKI estimation. Subsequently, the DKI-related parametric maps, including axial ($K_{//}$), radial ($K_{\perp}$), and mean kurtosis (MK), as well as the DTI-related parametric maps, including FA, axial ($D_{//}$), radial ($D_{\perp}$), and mean diffusivity (MD) were generated on a voxel-by-voxel basis using the method described previously.[18,20,24] The basic relationship among the diffusion-weighted signal intensity for a given diffusion direction as a function of the b value [S(b)], the apparent diffusion coefficient (D_{app}) as well as the apparent diffusional kurtosis (K_{app}) is shown in the following expression:

$$\ln\left(\frac{S(b)}{S(0)}\right) = -bD_{app} + \frac{1}{6}b^2D_{app}^2K_{app}^2$$

After derivation of all D_{app} and K_{app} values, the MK was calculated using the following expression:

$$MK = \frac{1}{n}\sum_{i=1}^{n}(K_{app})_i$$

where n is total number of directions along which the diffusion gradients were applied. The $K_{//}$ and $K_{\perp}$ were axial and radial diffusion kurtosis measured in the directions parallel and perpendicular to fiber orientation, respectively, using the following 2 expressions:

$K_{//} = K1$ and $K_{\perp} = (K2 + K3)/2$

where $K1$, $K2$, and $K3$ are diffusion kurtosis measured in 3 orthogonal axes of the diffusion tensor. In addition, the DTI-related FA was calculated using the following expression:

$$FA = \sqrt{\frac{3}{2}\frac{(\lambda_1 - MD)^2 + (\lambda_2 - MD)^2 + (\lambda_3 - MD)^2}{(\lambda_1^2 + \lambda_2^2 + \lambda_3^2)}},$$

where λ_1, λ_2, and λ_3 ($\lambda_1 > \lambda_2 > \lambda_3$) are 3 eigenvalues of a diffusion tensor fitted from all D_{app} values, and MD is the mean of these eigenvalues. The axial ($D_{//}$) and radial ($D_{\perp}$) diffusivities were computed using the following 2 expressions:

$D_{//} = \lambda_1$ and $D_{\perp} = (\lambda_1 + \lambda_2)/2$.

Moreover, the first eigenvector, which is in the long axis of a diffusion tensor, was utilized to generate color-encoded FA map by assigning red, green, and blue colors as left-to-right, anterior-to-posterior, and superior-to-posterior directions, respectively.

2.4. Tract-based ROI-selections

A tract-specific approach in selection of regions of interest (ROIs) was applied in this study in order to reduce influences from operator dependency and inter-subject differences. For this purpose, fiber-tracking was performed first using the MRtrix software package (Brain Research Institute, Melbourne, Australia, http://www.brain.org.au/software/) based on the constrained spherical deconvolution (CSD) method with the deterministic streamline algorithm[25,26] with the following criteria: radius of curvature >2 mm, step size = 0.2 mm, and tract lengths between 10 and 200 mm. As to the FA criteria, as various fiber tracts may pass through crossing regions with different degrees of diffusion anisotropy, this study used different FA thresholds as seeding and stopping criteria to trace different fiber tracts of the brain, which will be detailed in the next paragraphs. In this study, tract-based ROIs were placed on the corpus callosum (genu and splenium), bilateral cingulum, and motor-related tracts [corticospinal tract (CST) and corticobulbar tract (CBT)] to explore the association between DKI/DTI-related indices and early WM changes. These regions were confirmed individually by 2 experienced neuroradiologists (CYC and HWK, 28 and 10 years in imaging research experience, respectively) for each of the following ROI selections.

2.5. Corpus callosum

To delineate the trajectory of the corpus callosum, the central sagittal slice showing the most homogeneous appearance in shape on the colored FA maps was selected as a reference slice (Fig. 1 a). A polygonal ROI was manually drawn around the entire red color-marked corpus callosum that contains fiber tracts connecting both hemispheres of the brain. Fiber-tracking of the corpus callosum was subsequently performed on the selected ROI using FA thresholds of 0.6 and 0.3 as seeding and stopping criteria, respectively. The tracking result was illustrated in Fig. 1B with colored fiber tracts of the corpus callosum overlapped on a sagittal T1 image. In addition, an axial cross-section of the colored FA map that covers both genu and splenium of the corpus callosum was selected to draw 2 circular ROIs in the central portions of the genu and splenium of the corpus callosum, respectively (Fig. 1C). Afterwards, the mean DKI indices within the ROIs were calculated for statistical analysis.

2.6. Cingulum

Two circular ROIs were drawn above the corpus callosum on the colored FA maps for the delineation of the cingulum in each brain hemisphere. The sagittal slice of the colored FA maps that showed the most homogeneous appearance of the corpus callosum was identified. Accordingly, the first ROI was placed on the green-marked cingulum above the genu of the corpus callosum on a coronal slice of FA maps (Fig. 2A). For the second ROI, the sagittal and axial slice markers were used to approach the other end of the cingulum above the splenium of the corpus callosum on the corresponding coronal slice of the FA map, on which the second ROI was drawn (Fig. 2B). After performing fiber tracking using FA thresholds of 0.4 and 0.2 as seeding and stopping criteria, respectively, fiber tracts that passed through these 2 ROIs were retained as the cingulum fiber bundles superimposed on a sagittal T1 image (Fig. 2C). For statistical analysis of DKI indices, an axial cross-section of the colored FA map covering the bilateral cingulum was selected to draw 2 rectangular ROIs in both sides of the cingulum (Fig. 2D) within which the mean DKI indices were calculated.

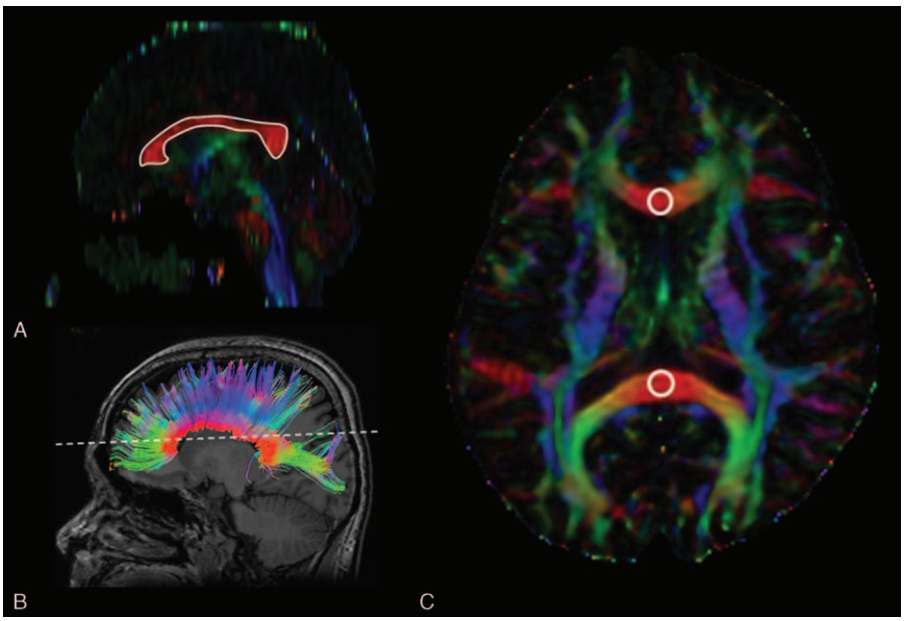

Figure 1. Tract-based ROI selection for the genu and splenium of the corpus callosum (GCC, SCC) in a normal subject. (A) A polygonal shaped ROI drawn over the CC in a sagittal colored FA map; (B) Trajectory of the CC tract overlapped on a sagittal T1 image; (C) Final ROIs of the GCC and SCC.

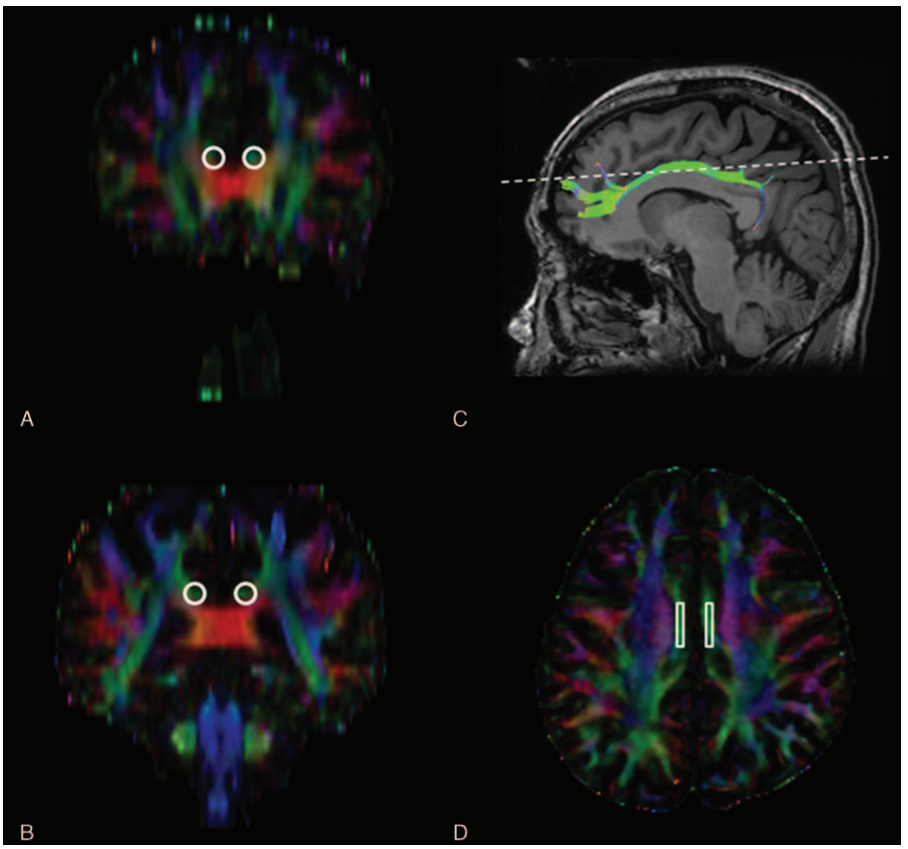

Figure 2. Tract-based ROI selection for the cingulum in a normal subject. (A) First, circular-shaped ROI drawn over the cingulum in a coronal colored FA map; (B) Second, circular-shaped ROI drawn over the cingulum in a coronal colored FA map; (C) Trajectory of the cingulum tract overlapped on a sagittal T1 image; (D) Final ROIs of the bilateral cingulum.

2.7. Corticospinal tract (CST)

Two ROIs were drawn on each cerebral hemisphere to identify CST. The first ROI was placed on the axial colored FA map at the level of the superior cerebral peduncle. A polygonal ROI was drawn around the purple part of the cerebral peduncle at each brain hemisphere (Fig. 3A). The second ROI was located in the pre-central centrum semiovales underneath the motor cortex using the axial FA image where the central sulcus was identified (Fig. 3B). CST was then traced with the fiber tracts passing through both ROIs using the same tracking criteria as those for cingulum bundles, with the results overlapped on a coronal T1 image (Fig. 3C). In addition, an axial cross-section of the colored FA map showing most of the bilateral ventricles was selected for drawing 2 circular ROIs that covered the regions of bilateral CST periventricularly (Fig. 3D). Subsequently, the mean DKI indices within these ROIs were calculated for statistical analysis.

2.8. Corticobulbar tract (CBT)

Similar to CST, 2 ROIs were drawn to identify CBT. As has been described in a previous report in CBT tracking,[27] the first ROI was placed on an axial T2-weighted image at the level of the superior cerebral peduncle as was for tracking CST (Fig. 4A). The second ROI with a leaf shape was drawn on lateral pre-central WM region in Brodmann 4 in another axial T2-weighted image at the level above the roof of the lateral ventricles (Fig. 4B). CBT was then traced with the fibers passing through both ROIs using FA thresholds of 0.2 and 0.1 as seeding and stopping criteria, respectively, again with results overlapped on a coronal T1 image (Fig. 4C). Afterwards, an axial cross-section of the colored FA map covering most of the orange-colored bilateral CBT was the selected to draw 2 ellipsoidal ROIs inside the regions of the CBT for the measurement of DKI indices (Fig. 4D).

2.9. Statistical analysis

All the data were analyzed using Statistical Package for the Social Science software, Version 20.0 (SPSS, Chicago, IL). Mean value and standard deviation (SD) of each DKI parameter from different ROIs were calculated first, and comparisons of the mean values between the patients with acute CO intoxication and normal controls were performed using the Mann–Whitney *U* test. The root-mean square average coefficient of variation (CV_{RMS}) and intraclass correlation coefficient (ICC) were calculated to assess the reproducibility of our proposed methods and CV_{RMS} values $<10\%$ and ICC >0.8 were interpreted as good. Spearman rank correlation test, a nonparametric test, was used to analyze the association between the carboxyhemoglobin levels and all DKI indices in the patient group. Correlations between smoking status of the patients and readouts of the DKI indices were examined by McNemar test. Multiple testing was corrected using the Benjamini–Hochberg method for false discovery rate,[28] with the corrected P value <0.05 to be considered statistically significant.

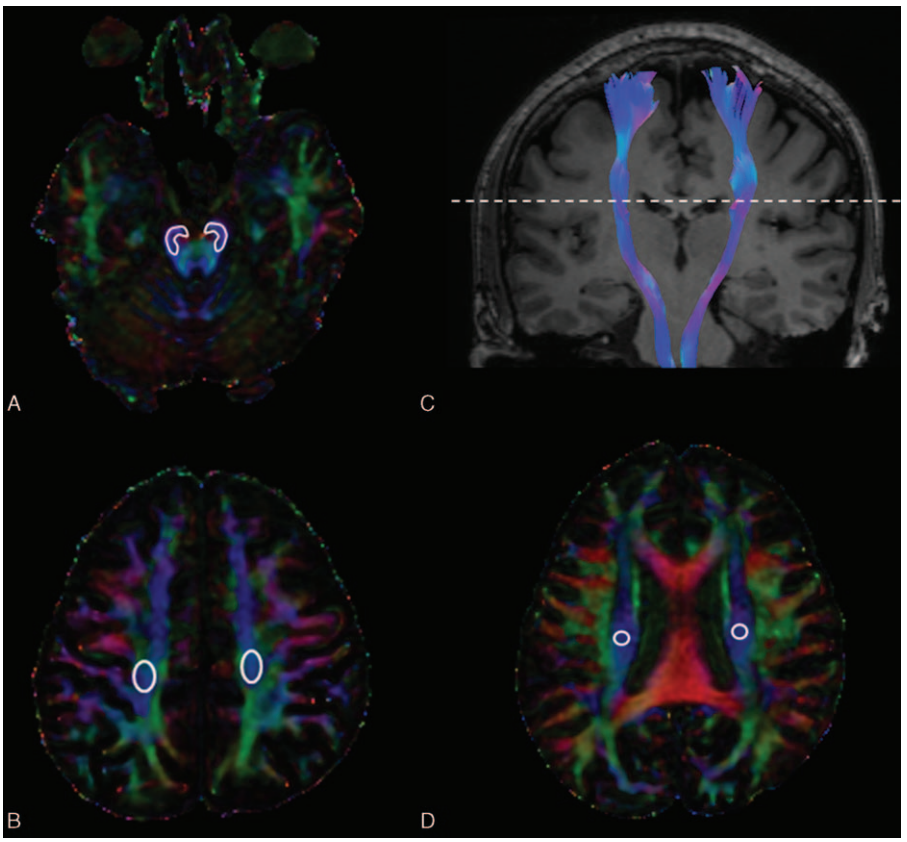

Figure 3. Tract-based ROI selection for the corticospinal tract (CST) in a normal subject. (A) First, polygonal-shaped ROIs placed on the cerebral peduncle in an axial colored FA map; (B) Second, ROI located in the centrum semiovales in the region of motor tracts; (C) Trajectory of the CST tract overlapped on a coronal T1 image; (D) Final ROIs of the bilateral CST.

3. Results

3.1. MR imaging findings

Conventional FLAIR, T2-weighted images, FA, and MK maps from a control subject and a 33-year-old woman with acute CO poisoning (COHb level = 19.9%; MR examination at the fourth day) were shown in Fig. 5. Although previous reports demonstrated that FLAIR and FA map could provide evidences of alterations in the brain WM at several weeks following CO exposure, no significant visual difference was found in these images obtained within 8 days after CO intoxication. On the contrary, a visually perceivable decrease of the MK value in the genu of corpus callosum was noticed in this representative patient (Fig. 5H, black arrow). Moreover, a better delineation of the caudate nuclei against lateral ventricles was found for the MK maps than the FA maps, likely due to artifactually decreased diffusion anisotropy of the periventricular gray matters from CSF contamination in the FA maps.[29] In contrast, DKI-related indices were less sensitive to CSF contamination than the conventional DTI-related indices,[30] leading to an improved visualization in the periventricular region.

3.2. DTI- and DKI-related parametric indices

The mean values and SD of the parametric indices derived from the abovementioned ROIs in the normal subjects and patients are presented in Fig. 6. In DTI-related measurements, the FA values were significantly decreased in the bilateral CST ($P_{corr} = 0.041$ and $P_{corr} = 0.046$, respectively) and the $D_{\perp}$ value were significantly increased in the right CST in patient group as compared with the control group ($P_{corr} < 0.049$). The remaining other ROIs other than CST showed no significant differences between patent and control groups in terms of FA and $D_{\perp}$ and $D_{//}$ values examined (all $P_{corr} > 0.05$). In DKI-related measurements, on the contrary, significant differences of MK values were shown in the genu of corpus callosum ($P_{corr} = 0.004$), right cingulum ($P_{corr} = 0.008$), and bilateral CST ($P_{corr} = 0.020$ and $P_{corr} = 0.025$, respectively) and CBT ($P_{corr} = 0.006$ and $P_{corr} = 0.007$, respectively) in the patients with acute CO intoxication as compared with control subjects. No significant differences in $K_{//}$ values were found (all $P_{corr} > 0.05$). Significant decreases of the $K_{\perp}$ values were shown in the genu of corpus callosum, right cingulum, right CST, and left CBT in patient groups (all $P_{corr} < 0.05$). DKI parameters demonstrated substantially more regions of WM abnormality in acute CO poisoning patients than did the DTI parameters. Moreover, the CV_{RMS} and ICC of the 2-session measurements in the selected ROIs on the normal subjects were less than 9% and greater than 0.8, respectively, indicating good reproducibility (Table 1).

3.3. Correlation between the MK values and the carboxyhemoglobin levels

Although the MK values of the right and left cingulum and CSTs showed the trend of correlation with the COHb levels, the relationship failed to reach statistical significance after correction

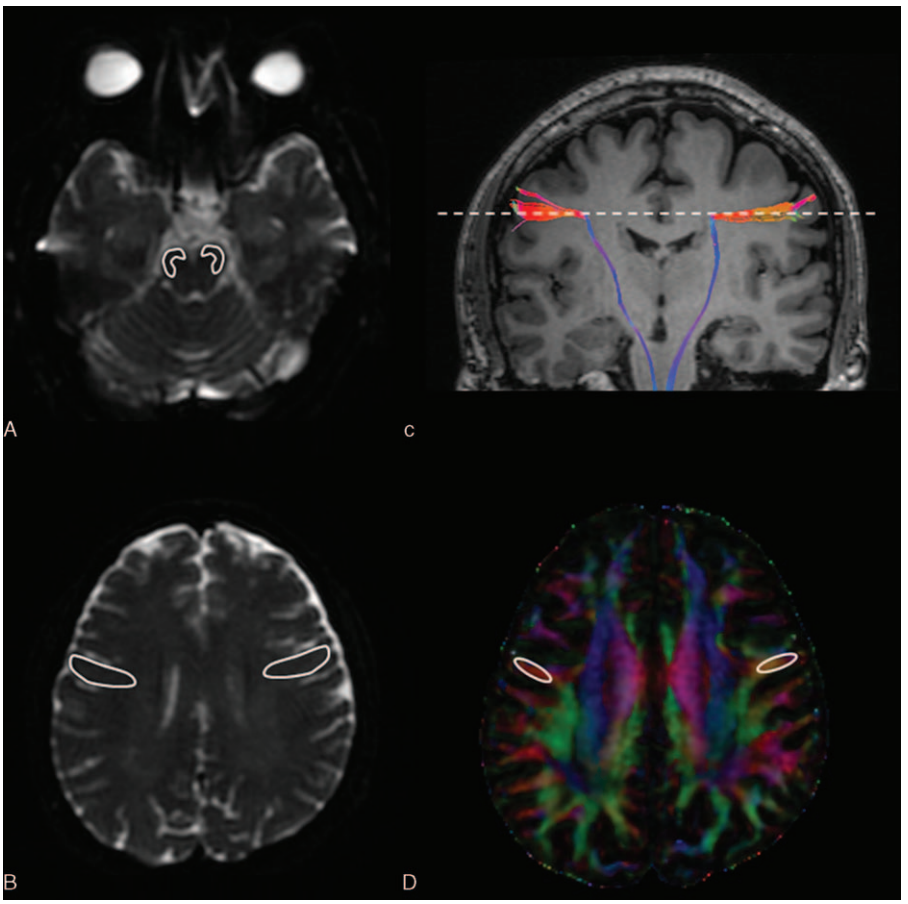

Figure 4. Tract-based ROI selection for the corticobulbar tract (CBT) in a normal subject. (A) First, polygonal-shaped ROI were placed on the cerebral peduncle in a axial T2-weighted image; (B) Second, ROI with a leave shape located on the superior frontal subcortical regions at the level of the lateral ventricular roof in an axial T2-weighted image; (C) Trajectory of the CBT overlapped on a coronal T1 image; (D) Final ROIs of the bilateral CBT.

for multiple comparison ($r=0.591$, $P_{corr}=0.0594$, $r=0.636$, $P_{corr}=0.0594$, $r=0.600$, $P_{corr}=0.0594$, $r=0.709$, $P_{corr}=0.0594$, respectively) (Table 2). In addition, no significant correlations were seen between MK and COHb in the genu of corpus callosum, splenium of corpus callosum, and bilateral CBTs ($r=-0.073$, $P_{corr}=0.5042$, $r=0.127$, $P_{corr}=0.5013$, $r=0.127$, $P_{corr}=0.5013$, $r=0.000$, $P_{corr}=0.5303$, respectively) (Table 2). As to the other DTI- and DKI-related indices, no significant correlations with COHb levels were found. Moreover, there were no significant correlations between the smoking status of the patients and readouts of the DKI indices.

4. Discussion

Our results further prove that DKI may potentially play an important role, as compared with conventional MRI, in the assessment of acute brain injury following CO poisoning. Previously, studies have shown hyperintensity changes of the periventricular WM and centrum semiovales on conventional T2-weighted and FLAIR images in acute CO-induced brain injuries, although questions remain whether those normal-appearing white matters are unaffected by the toxic process, as most of our patients showed unremarkable finding in conventional MRI.[9,31] Because conventional MRI is insensitive to acute white matter injury in CO intoxication, DTI-related indices have emerged and proposed as surrogate biomarkers in identifying brain demyelination following CO intoxication and predicting clinical outcome of the patients.[14] Notwithstanding, the non-Gaussian DKI could offer an improved sensitivity in revealing neural microstructure changes due to ischemic stroke or multiple sclerosis,[32,33] our study further proved that DKI is superior to DTI in detecting early CO-induced white matter injury. To the best of our knowledge, our study is the first DKI investigation to assess the WM abnormalities of the acute CO patients.

Previous study has shown diffuse decrease in WM FA at a later stage in patients 1 to 2 months following CO intoxication.[14] Our results showed only limited regions of FA decreases in the acute stage of CO exposure. This could be understood because the increases of water diffusivity and decreases of FA value may only reveal an increase of the extracellular volume and/or possibly altered fiber integrity due to demyelination and axonal loss. These DTI-related indices based on a Gaussian assumption provide only limited information about tissue microstructural property.[34] In DKI, the kurtosis excess is a fourth central moment of water displacement distribution that provides information about the deviation of the water diffusion displacement profile, thus allowing a more comprehensive characterization of the diffusion properties of neural tissues. This explains why the extents of WM abnormalities identified from MK maps were observed much more extensive than those seen in DTI image. In our results, significant decreases of MK values in the genu of corpus callosum, right cingulum, bilateral CST, and CBT

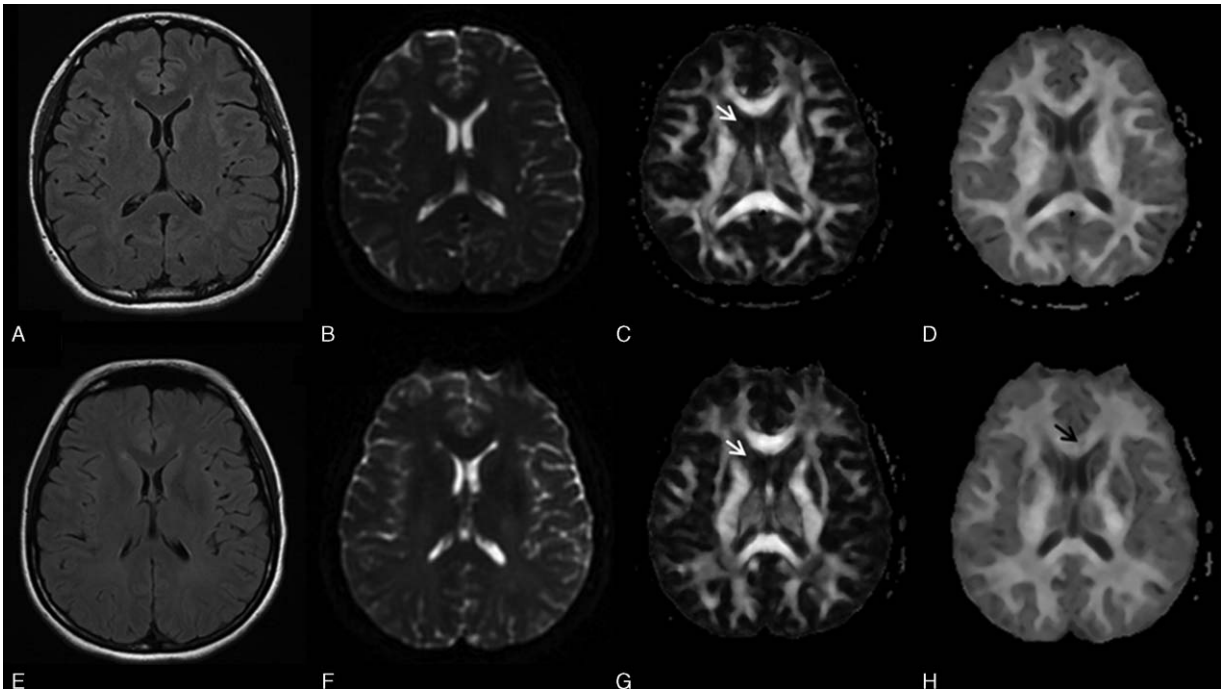

Figure 5. Conventional FLAIR, T2-weighted images, FA and MK maps from a control subject (A–D) and a 33-year-old woman with acute CO poisoning (E–H) were shown. No visually perceivable differences were found in the FLAIR, T2-weighted images, and FA maps between the patient and control. A noticeable hypointensity region was displayed in the genu of corpus callosum on MK map in the representative patient (black arrow). Furthermore, delineation between the caudate nuclei and the lateral ventricles was superior on the MK maps as compared with FA maps (white arrows).

were observed after CO poisoning. A decrease in MK value may be more likely associated with neuronal shrinkage and degenerative change, reflecting a reduction in diffusional heterogeneity, suggesting that the MK value could be a more sensitive biomarker for early detection of encephalopathy in patients with CO intoxication than the conventional DTI-related indices. Moreover, directional kurtosis indices derived from the kurtosis tensor model have been demonstrated in an animal study that the indices change may provide additional information possibly related to the pathological process in the membranes of the glial cells, astrocytes, and oligodendrocytes, rather than the myelin sheath alone.[18] Our results also showed significant differences of $K_{\perp}$ values in several ROIs between the patient and control groups, which further emphasizes the superiority of diffusion kurtosis measurements over the DTI method.

WM demyelination has been recognized as the principal feature of the delayed encephalopathy after CO poisoning in pathological findings,[35] which are intimately associated with neurological sequelae. Damage to the periventricular WM structures, such as corpus callosum and cingulate as revealed by the reduced MK in our study, was indicated to be mainly linked with cognitive function deficits and memory impairment.[36] Although the underlying pathological mechanism needs more investigation, degradation of myelin basic protein, the major myelin protein of central nervous system, and microglial activation were observed in rats after CO poisoning.[37] Two recent reports demonstrated the histological correlations between DKI-related indices and WM changes in a mouse model of cuprizone-induced demyelination,[22,23] where the association between diffusion kurtosis and myelin loss as well as decrease in axonal water fraction was established. As such, alterations of DKI-related indices are believed to be linked to a loss of microstructure and the relevant pathological process, such as reactive astrogliosis. In the present study, among all parameters investigated, MK and $K_{\perp}$ values showed the highest sensitivity for early detection of WM changes in the genu of corpus callosum and right cingulum in the acute CO patients, suggesting that these DKI-related indices may be capable of predicting the possibility of the delayed encephalopathy, including cognitive function deficits, after CO poisoning.

The pathophysiology related to the development of delayed encephalopathy remains unclear. The clinical metrics for evaluating the severity of CO intoxication that leads to different neuropsychological symptoms can be completely unpredictable.[38] Elevated CO blood levels are thought to be associated with reduced cellular oxygen metabolism and lipid peroxidation, which could result in brain damage ultimately. However, no significant correlation between the carboxyhemoglobin levels and the development of delayed neuropsychological sequelae of the patients was found in a retrospective study.[38] Our study was in concert with the previous reports that no significant correlations between the MK values and the carboxyhemoglobin levels could be established.

Manual ROI-based analysis has been used in several DTI studies to detect WM changes related to the delayed encephalopathy in patients with CO intoxication.[12,14] However, these studies might raise the questions of possible subjective discrepancies due to operator dependency. On the contrary, tract-specific analysis has been demonstrated as a reliable approach to assess WM integrity objectively, with which information of diffusion tractography is used to guide the quantification of the DTI-related indices on a specific fiber tract bundle.[39,40] In the present study, we used the tract-specific approach in conjugation with the ROI analysis to explore the early WM abnormalities,

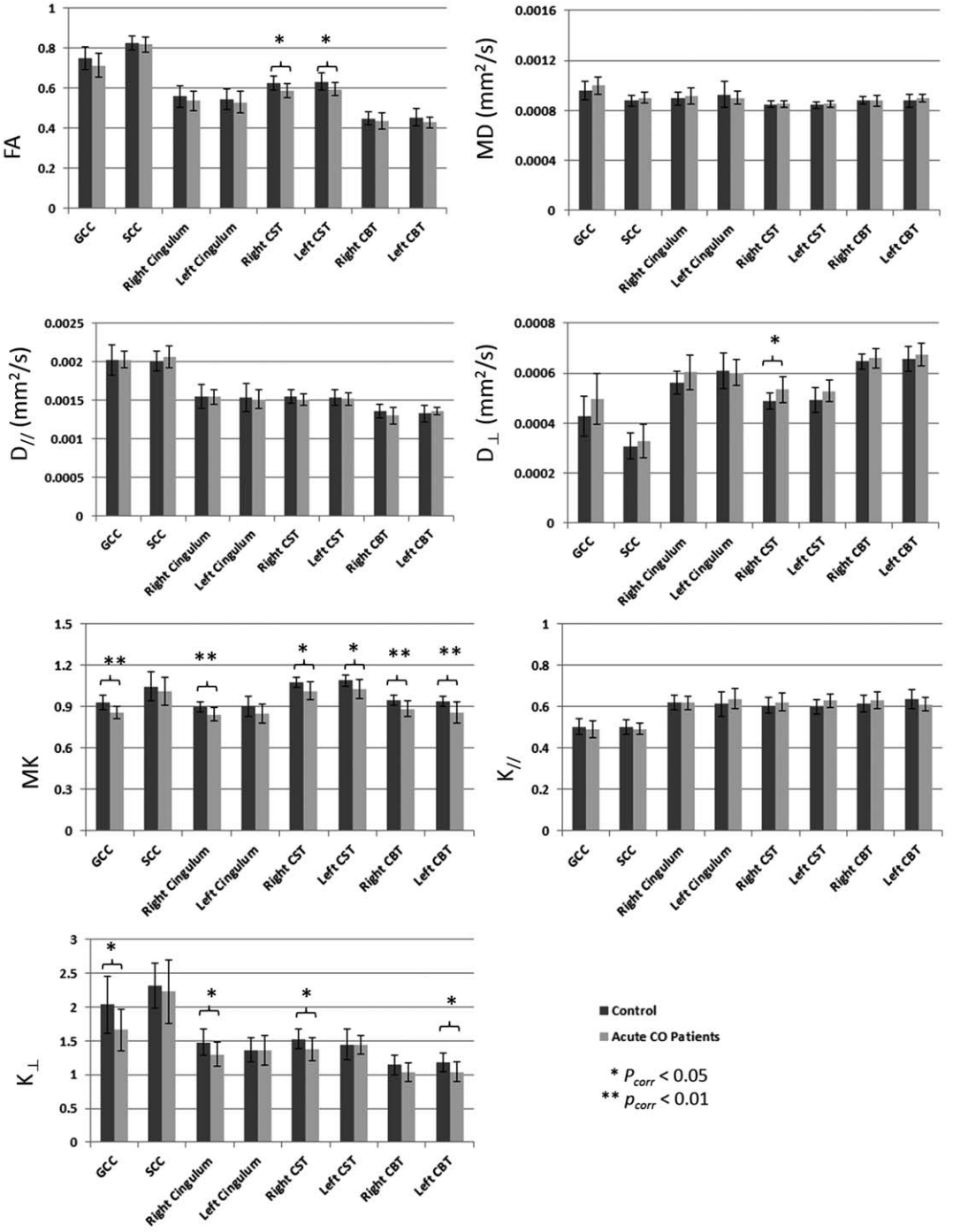

Figure 6. Mean and standard deviation (SD) of the DT- and DK-related indices derived over the ROIs of the genu and splenium of corpus callosum (GCC, SCC), the bilateral cingulum, corticospinal tract (CST), and corticobulbar tract (CBT) in control and acute CO patients. Significant differences with respect to controls were indicated by $^{*}P_{corr} < 0.05$ and $^{\dagger}P_{corr} < 0.01$. $D_{//}$ = axial diffusivity; $D_{\perp}$ = radial diffusivity; FA = fractional anisotropy; $K_{//}$ = axial kurtosis; $K_{\perp}$ = radial kurtosis; MD = mean diffusivity; MK = mean kurtosis.

which could provide more specific and flexible comparisons, especially in tracts that are hard to identify. For instance, using this tract-based analytic method to assess early changes of the motor tracts may provide information with differentiable functions such as CBT alterations for masked facies or CST damages for gait disturbance, both being predominant features of Parkinsonism after CO intoxication.

In addition to DTI and DKI techniques, T2 relaxation based myelin water imaging, measuring myelin water fraction (MWF), can be an alternative to assess subtle changes on the patients with demyelinating diseases, such as multiple sclerosis.[41] Although obtaining whole-brain MWF maps could be time-consuming and its accuracy can be subject to the image quality, a good relationship between derived MWF and histological results has

Table 1

The root-mean square average coefficient of variation (CV_{RMS}) and intraclass correlation coefficient (ICC) in the genu and splenium of corpus callosum (GCC, SCC), the bilateral cingulum, corticospinal tract (CST), and corticobulbar tract (CBT) in the normal subjects of the reproducibility test.

	CV_{RMS} (%)	ICC
GCC	6.82	0.96
SCC	6.02	0.91
Right cingulum	8.60	0.81
Left cingulum	4.99	0.98
Right CST	3.29	0.97
Left CST	4.86	0.93
Right CBT	8.14	0.89
Left CBT	3.55	0.96

been demonstrated in postmortem and animal studies.[42] Consequently, a combination of DKI and myelin water imaging may elucidate the underlying biomechanism of WM demyelination after CO intoxication.

There are several limitations in our study. First, enrollment of acute CO-intoxicated patients for MRI study was difficult. This resulted in a small sample size, thus leading to a limited statistical power. Further investigations with broader samples may be needed to confirm our observation. Second, DKI measurements in the present study were executed only at the early stage after CO exposure. A longitudinal study including comprehensive monitoring of the temporal evolution of the DKI-related indices and evaluation of the clinical symptoms should be useful in the interpretation of the neurophysiological changes. In addition, a direct correlation between the diffusional kurtosis indices and the pathological changes of WM injury after CO intoxication has not been conclusive. For these reasons, the results should be carefully interpreted, as only changes in the acute stage were studied. Another penalty of losing image fidelity could result from the application of pre-processing median filter. Using a noise robust spatially regularized algorithm proposed by Kumar et al[42] could be a potential remedy. Finally, the spatial resolution in the present study is limited due to the relatively longer acquisition time of the DKI technique for humans, which may restrict further identification of subtle WM alterations after CO exposure. A translational study taking advantage of high-resolution MRI in a rat model could provide a remedy as well as the histological confirmation.

In conclusion, DKI could provide more information, such as directional and MK, than does the conventional DTI, thus could contribute to the early detection of cerebral microstructural changes and may help predict the late complications such as delayed encephalopathy in patients after CO intoxication. Further investigations using the diffusional kurtosis approach could improve early diagnosis and treatment strategies for CO-induced delayed encephalopathy.

Table 2

Correlations between the MK values in the genu and splenium of corpus callosum (GCC, SCC), the bilateral cingulum, corticospinal tract (CST), and corticobulbar tract (CBT) with the carboxyhemoglobin levels in the acute CO patients.

	Correlation coefficient	*P*
GCC	−0.073	0.5042
SCC	0.127	0.5013
Right cingulum	0.591	0.0594
Left cingulum	0.636	0.0594
Right CST	0.600	0.0594
Left CST	0.709	0.0594
Right CBT	0.127	0.5013
Left CBT	0.000	0.5303

References

[1] Chang SS, Gunnell D, Wheeler BW, et al. The evolution of the epidemic of charcoal-burning suicide in Taiwan: a spatial and temporal analysis. PLoS Med 2010;7:e1000212.

[2] Kuroda H, Fujihara K, Takahashi S, et al. A case of delayed encephalophathy after carbon monoxide poisoning longitudinally monitored by diffusion imaging. AJNR Am J Neuroradiol 2012;33:52–4.

[3] Lee MS, Marsden CD. Neurological sequelae following carbon monoxide poisoning clinical course and outcome according to the clinical types and brain computed tomography scan findings. Mov Disord 1994;9:550–8.

[4] Senol MG, Yildiz S, Ersanli D, et al. Carbon monoxide-induced cortical visual loss: treatment with hyperbaric oxygen four years later. Med Princ Pract 2009;18:67–9.

[5] Kao LW, Nanagas KA. Toxicity associated with carbon monoxide. Clin Lab Med 2006;26:99–125.

[6] Silver DA, Cross M, Fox B, et al. Computed tomography of the brain in acute carbon monoxide poisoning. Clin Radiol 1996;51:480–3.

[7] Gale SD, Hopkins RO, Weaver LK, et al. MRI, quantitative MRI, SPECT, and neuropsychological findings following carbon monoxide poisoning. Brain Inj 1999;13:229–43.

[8] Choi IS. Parkinsonism after carbon monoxide poisoning. Eur Neurol 2002;48:30–3.

[9] Lo CP, Chen SY, Lee KW, et al. Brain injury after acute carbon monoxide poisoning: early and late complications. AJR 2007;189:205–11.

[10] Vila JF, Meli FJ, Serqueira OE, et al. Diffusion tensor magnetic resonance imaging: a promising technique to characterize and track delayed encephalopathy after acute carbon monoxide poisoning. Undersea Hyperb Med 2005;32:151–6.

[11] Lo CP, Chen SY, Chou MC, et al. Diffusion-tensor MR imaging for evaluation of the efficacy of hyperbaric oxygen therapy in patients with delayed neuropsychiatric syndrome caused by carbon monoxide inhalation. Eur J Neurol 2007;14:777–82.

[12] Lin WC, Lu CH, Lee YC, et al. White matter damage in carbon monoxide introxication assessed in vivo using diffusion tensor MR imaging. AJNR Am J Neuroradiol 2009;30:1248–55.

[13] Chang CC, Lee YC, Chang WN, et al. Damage of white matter tract correlated with neuropsycological deficits in carbon monoxide intoxication after hyperbaric oxygen. J Neurotrauma 2009;26:1263–70.

[14] Hou X, Ma L, Wu L, et al. Diffusion tensor imaging for predicting the clinical outcome of delayed encephalophathy of acute carbon monoxide poisoning. Eur Neurol 2013;69:275–80.

[15] Niendorf T, Dijkhuizen RM, Norris DG, et al. Biexponential diffusion attenuation in various states of brain tissue: implications for diffusion in brain tissue. Magn Reson Med 1996;36:847–57.

[16] Mulkern RV, Zengingonul HP, Robertson RL, et al. Multi-component apparent diffusion coefficients in human brain: relationship to spin-lattice relaxation. Magn Reson Med 2000;44:292–300.

[17] Assaf Y, Mayk A, Cohen Y. Displacement imaging of spinal cord using q-space diffusion-weighted MRI. Magn Reson Med 2000;44:713–22.

[18] Hui ES, Cheung MM, Qi L, et al. Towards better MR characterization of neural tissues using directional diffusion kurtosis analysis. Neuroimage 2008;42:122–34.

[19] Jensen JH, Helpern JA. MRI quantification of non-Gaussian water diffusion by kurtosis analysis. NMR Biomed 2010;23:698–710.

[20] Wu EX, Cheung MM. MR diffusion kurtosis imaging for neural tissue characterization. NMR Biomed 2010;23:836–48.

[21] Jensen JH, Helpern JA, Ramani A, et al. Diffusion kurtosis imaging: the quantification of non-Gaussian water diffusion by means of magnetic resonance imaging. Magn Reson Med 2005;53:1432–40.

[22] Falangola MF, Guifoyle DN, Tabesh A, et al. Histological correlation of diffusional kurtosis and white matter modeling metrics in cuprizone-induced corpus callosum demyelination. NMR Biomed 2014;27:948–57.

[23] Guglielmetti C, Veraart J, Roelant E, et al. Diffusion kurtosis imaging probes cortical alterations and white matter pathology following

cuprizone induced demyelination and spontaneous remyelination. Neuroimage 2016;125:363–77.
[24] Tabesh A, Jensen JH, Ardekani BA, et al. Estimation of tensors and tensor-derived measures in diffusional kurtosis imaging. Magn Reson Med 2011;65:823–36.
[25] Tournier JD, Calamante F, Connelly A. MRtrix: diffusion tractography in crossing fibre regions. Int J Imaging Syst Technol 2012;22:53–66.
[26] Tournier JD, Calamante F, Connelly A. Robust determination of the fibre orientation distribution in diffusion MRI: non-negativity constrained super-resolved spherical deconvolution. Neuroimage 2007;35: 1459–72.
[27] Bucci M, Mandelli ML, Berman JI, et al. Quantifying diffusion MRI tractography of the corticospinal tract in brain tumors with deterministic and probabilistic methods. Neuroimage 2013;367–8. Clinical 3.
[28] Storey JD. A direct approach to false discovery rates. J R Statist Soc B 2002;64(Part 3):479–98.
[29] Ma X, Kadah YM, LaConte SM, et al. Enhancing measured diffusion anisotropy in gray matter by eliminating CSF contamination with FLAIR. Magn Reson Med 2004;51:423–7.
[30] Yang AW, Jensen JH, Hu CC, et al. Effect of cerebral spinal fluid suppression for diffusional kurtosis imaging. J Magn Reson Imag 2013;37:365–71.
[31] Beppu T. The role of MR imaging in assessment of brain damage from carbon monoxide poisoning: a review of the literature. AJNR Am J Neuroradiol 2014;35:625–31.
[32] Raz E, Bester M, Sigmund EE, et al. A better characterization of spinal cord damage in multiple sclerosis: a diffusional kurtosis imaging study. Spine 2013;34:1846–52.
[33] Hui ES, Fieremans E, Jensen JH, et al. Stroke assessment with diffusional kurtosis imaging. Stroke 2012;43:2968–73.
[34] Nijeholt GJ, Bergers E, Kamphorst W, et al. Post-mortem high-resolution MRI of the spinal cord in multiple sclerosis: a correlative study with conventional MRI, histopathology and clinical phenotype. Brain 2001;124:154–66.
[35] Lapresle J, Fardeau M. The central nervous system and carbon monoxide poisoning. II. Anatomical study of brain lesions following intoxication with carbon monoxide (22 cases). Prog Brain Res 1967;24:31–74.
[36] Schmahmann JD, Smith EE, Eichler FS, et al. Cerebral white matter: neuroanatomy, clinical neurology, and neurobehavioral correlates. Ann N Y Acad Sci 2008;1142:266–309.
[37] Thom SR, Bhopale VM, Fisher D, et al. Delayed neuropathology after carbon monoxide poisoning is immune-mediated. Proc Natl Acad Sci U S A 2004;101:13660–5.
[38] Ku HL, Yang KC, Lee YC, et al. Predictors of carbon monoxide poisoning-induced delayed neuropsychological sequelae. Gen Hosp Psychiatry 2010;32:310–4.
[39] Kanaan RA, Shergill SS, Barker GJ, et al. Tract-specific anisotropy measurements in diffusion tensor imaging. Psychiatry Res 2006;146: 73–82.
[40] Tang PF, Ko YH, Luo ZA, et al. Tract-specific and region of interest analysis of corticospinal tract integrity in subcortical ischemic stroke: reliability and correlation with motor function of affected lower extremity. AJNR Am J Neuroradiol 2010;31:1023–30.
[41] Prasloski T, Rauscher A, MacKay AL, et al. Rapid whole cerebrum myelin water imaging using a 3D GRASE sequence. Neuroimage 2012;63:533–9.
[42] Kumar D, Siemonsen S, Heesen C, et al. Noise robust spatially regularized myelin water fraction mapping with the intrinsic B1-error correction based on the linearized version of the extended phase graph model. J Magn Reson Imaging 2016;43:800–17.